Draft version October 8, 2010
Preprint typeset using LaTeX style emulateapj v. 12/14/05

THE COMPOSITE SPECTRUM OF STRONG LYMAN-ALPHA FOREST ABSORBERS

Matthew M. Pieri[1,2], Stephan Frank[3], David H. Weinberg[1,4], Smita Mathur[1], and Donald G. York[5,6]

Draft version October 8, 2010

ABSTRACT

We present a new method for probing the physical conditions and metal enrichment of the Intergalactic Medium: the composite spectrum of Lyα forest absorbers. We apply this technique to a sample of 9480 Lyα absorbers with redshift $2 < z < 3.5$ identified in the spectra of 13,279 high-redshift quasars from the Sloan Digital Sky Survey (SDSS) Fifth Data Release (DR5). Absorbers are selected as local minima in the spectra with $2.4 < \tau_{\rm Ly\alpha} < 4.0$; at SDSS resolution ($\approx 150\,{\rm km\,s^{-1}}$ FWHM), these absorbers are blends of systems that are individually weaker. In the stacked spectra we detect seven Lyman-series lines and metal lines of O VI, N V, C IV, C III, Si IV, C II, Al II, Si II, Fe II, Mg II, and O I. Many of these lines have peak optical depths of < 0.02, but they are nonetheless detected at high statistical significance. Modeling the Lyman-series measurements implies that our selected systems have total H I column densities $N_{\rm HI} \approx 10^{15.4}{\rm cm}^{-2}$. Assuming typical physical conditions $\rho/\bar{\rho} = 10$, $T = 10^4 - 10^{4.5}\,{\rm K}$, and [Fe/H]$= -2$ yields reasonable agreement with the line strengths of high-ionization species, but it underpredicts the low-ionization species by two orders of magnitude or more. This discrepancy suggests that the low ionization lines arise in dense, cool, metal-rich clumps, present in some absorption systems.

Subject headings: galaxies: formation — intergalactic medium — quasars: absorption lines

1. INTRODUCTION

The Lyman-α forest is a tracer of the diffuse matter between galaxies known as the Intergalactic Medium (IGM), and at high redshift ($2 < z < 4$) this diffuse medium contains roughly 70% of the baryonic mass and occupies 90% or more of the volume. Galaxies form from the collapse of dark matter structures and corresponding accretion of gas from the IGM. But this is not a one-way process, and feedback is vital for a complete picture. Galactic outflows modify the kinetic and thermal energy of the medium and distribute the by-product of star formation: metals (e.g. Mac Low & Ferrara 1999; Madau et al. 2001; Oppenheimer & Davé 2006; Pieri et al. 2007; Pieri & Martel 2007).

Metals have been observed in the high redshift Lyα forest. In particular C IV (e.g. Meyer & York 1987; Cowie et al. 1995; Songaila & Cowie 1996; Ellison et al. 2000; Schaye et al. 2003; Pieri et al. 2006) and O VI (e.g. Schaye et al. 2000; Pieri & Haehnelt 2004; Simcoe et al. 2004; Bergeron & Herbert-Fort 2005; Aguirre et al. 2008; Frank et al. 2010; Pieri et al. 2010) provide prominent absorbers and are commonly measured. Other species seen are Si IV, Si III, C III and N V (e.g. Schaye et al. 2003; Aguirre et al. 2004; Fechner & Richter 2009). These measurements provide some indications of the regions of the Universe touched by mechanical feedback, but they can also provide a useful probe of the ionization properties of the medium (and so the physical conditions of the gas), and the abundance pattern. The main obstacle to significant progress on the latter two goals is a lack of large numbers of metal species to measure both from the same element (to measure ionization characteristics) and from different elements (to measure abundance patterns).

In this paper, we introduce a new technique for the detection of weak metal lines — the composite spectrum of Lyα forest absorbers. We apply this approach to the largest Lyα forest dataset available: the Sloan Digital Sky Survey (SDSS) sample of QSO spectra. Pieri et al. (2010) demonstrated that the SDSS sample can provide precision measurements of weak lines by searching for O VI absorption associated with the bulk of the Lyα forest. Here we produce a blind search for absorption correlated with the strong Lyα forest absorbers; we identify and fit 19 metal lines.

2. PRODUCTION OF COMPOSITE SPECTRA

2.1. *The Sample and Lyman-α Forest Line Selection*

We use the Sloan Digital Sky Survey Data Release 5 (SDSS DR5) (Adelman-McCarthy et al. 2007), which provides 13,279 QSOs with useful forest coverage in the redshift range $2 < z < 3.5$. The spectra are taken from the QSO Absorption Line Sample (QSOALS; York et al. 2006) in the same manner described in Pieri et al. (2010) employed for DR3 spectra. The spectral resolution is wavelength dependent and varies from $R = 1800 - 2200$. In the following work we assume that $R = 2000$ at all wavelengths, and the error introduced by this approximation is smaller than the quoted errors.

We define "absorbers" in a simple way, selecting pixels that are lower in flux than their two neighboring pixels and have optical depth $2.4 < \tau_{\rm Ly\alpha} < 4$. We require

[1] Department of Astronomy, The Ohio State University, 140 West 18th Avenue, Columbus, OH 43210, USA
[2] CASA, Department of Astrophysical and Planetary Sciences, University of Colorado, 389 UCB, Boulder, CO 80309, USA; mpieri@colorado.edu
[3] Observatoire Astronomique de Marseille-Provence, Pôle de l'Étoile Site de Chteau-Gombert, 38, rue Frédéric Joliot-Curie 13388 Marseille cedex 13, France
[4] Institute for Advanced Study, Einstein Drive, Princeton, NJ 08540
[5] Department of Astronomy and Astrophysics, University of Chicago, Chicago, IL 60637, USA
[6] Enrico Fermi Institute, University of Chicago, Chicago, IL 60637, USA

that our Lyα absorbers are redward of the Lyβ forest and blueward of 5000 $\mathrm{km\,s^{-1}}$ from the quasar Lyα emission redshift. In the stacked spectrum discussed in this paper we use only Lyα absorbers in the redshift range $2 < z < 3.5$, resulting in some variation in the average redshift across the stacked spectrum (see Figure 1). We ensure that the selected absorbers are not saturated at SDSS resolution by requiring a minimum flux of $\sigma_n/2$. This requirement, which eliminates damped Lyα systems and noisy lines, discards 86% of Lyα absorbers in the required optical depth range. At SDSS spectral resolution, solitary Lyα forest lines with $b-$parameters $\sim 30\,\mathrm{km\,s^{-1}}$ and no damping wings do not reach an apparent optical depth greater than $\tau_{\mathrm{Ly}\alpha} \approx 1.9$, even if they are fully saturated. The absorption features in our sample are therefore blends of several Lyα forest lines rather than individual strong lines; we address the typical column densities of these features in §3 below, using the stacked spectra themselves.

2.2. *Spectral Stacking Methodology*

For each Lyα absorber in our sample, we de-redshift the whole spectrum to its rest-frame. Each quasar spectrum is carried forward once for every Lyα absorber, so some SDSS spectra are used more than once while others are not used at all. What results is a stack of spectra on a rest-frame wavelength grid. We employ two statistics to produce composite spectra: the median, and the arithmetic mean with a 3% outlier clipping. We require a minimum of 100 pixels for the measurement of the stacked spectrum at any point. When computing the composite spectrum redward of 1236Å, we only include pixels if they are outside of the Lyα forest of the quasar spectrum in question, since the pixels outside of the forest have much less background absorption and associated random fluctuations.

We estimate the error in the flux for the stacked spectrum by bootstrapping the data using 100 realizations. This is mostly consistent with the estimate from the propagation of errors, but it is larger in the wavelength range between the Lyβ and Lyα lines, due to scatter in uncorrelated Lyα forest absorption.

Figure 1 shows the stacked spectrum we obtain using the median (which is our fiducial choice). The stacked spectrum never reaches 100% transmission ($F = 1$) because there is always some uncorrelated, contaminating absorption.

2.3. *Composite Spectra of Lyman-α Forest Absorbers*

The full-width-half-maximum of SDSS resolution is $136 - 167$ $\mathrm{km\,s^{-1}}$, which corresponds to an effective Doppler parameter of $b_{\mathrm{SDSS}} = 82 - 100$ $\mathrm{km\,s^{-1}}$. This is around four times as broad as typical Lyman-series lines and broader still for metal lines. Hence the majority of contaminating "background" absorption in our spectra is not a true superposition of overlapping lines but a blending of distinct lines that appear superimposed due to SDSS resolution.

Given that uncorrelated contaminating absorption varies smoothly in our stacked spectrum, we can treat it as a continuum by performing a standard spline fit, producing the 'pseudo-continuum' shown by the overlay in Figure 1. We have scaled away its effect by adding the flux decrement of the pseudo-continuum to our stacked spectrum, thus arriving at what is effectively a composite rest-frame spectrum of the selected Lyα absorbers.

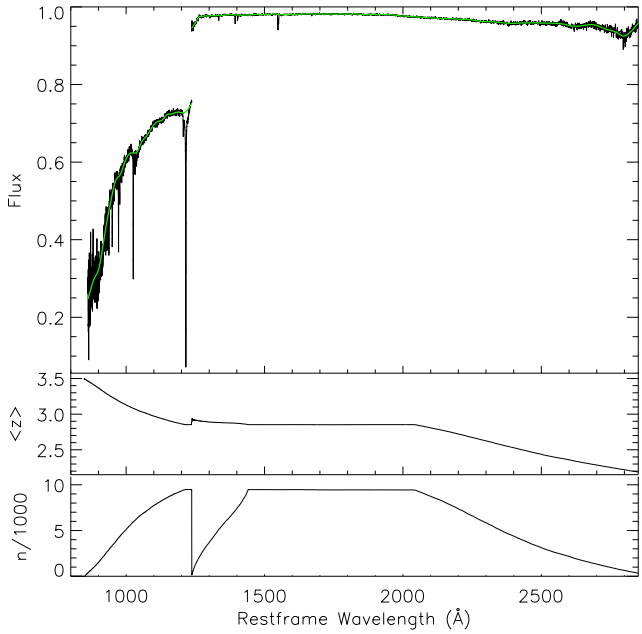

FIG. 1.— *Top panel*: The median stacked spectrum of 9480 Lyα absorbers. Overlaid in green is the 'pseudo-continuum' set by uncorrelated absorption. Lyman series lines and other lines can be seen along with a broad absorption trough caused by uncorrelated Lyman series lines. *Middle panel*: The mean redshift of pixels that make up the stacked spectrum. *Bottom panel*: The number of pixels that go into the stacked spectrum at every wavelength.

Figure 2 shows the median spectral stack of our sample of Lyα forest absorbers renormalized using the pseudo-continuum. A great many absorption lines are seen in this composite rest-frame spectrum. The Lyman series is particularly clear and is marked by dotted lines. Numerous metal lines are also seen at high confidence and are marked with dashed lines and labelled.

The Lyα line shows large wings, which are to be expected as a signal of large scale structure. The scale of the correlation extends to $\sim 3000\,\mathrm{km\,s^{-1}}$, which is in good agreement with the findings of McDonald et al. (2006). There is no indication that the signal arises from damping wings, and higher order Lyman lines rule out this interpretation (see following section). These wings have not been carefully fitted to separate the signal of clustering from the mean flux decrement in the forest, as the measurements in this paper are not dependent on this fit.

It should be noted that the weak lines seen redward of some lines (e.g. O VI, Si IV, and C IV doublets) are a signal due to Si III interlopers. There is a small sample of strong Si III absorbers that has entered our sample of Lyα lines for stacking. When these lines are misinterpreted as Lyα, a "shadow" signal in our stacked spectra is seen shifted by $\lambda_{\mathrm{Ly}\alpha}/\lambda_{\mathrm{SiIII}} = 1216/1206$. This shadowing is apparent for every identified metal line in the arithmetic mean stack, in keeping with its status as a less outlier-resistant statistic. We disregard these "shadow" lines in our analysis below. It is surprising that no substantial shadow is seen for Lyα; we do not have a simple explanation for this effect, and it appears that these Si III absorbers are an interesting sample in their own right.

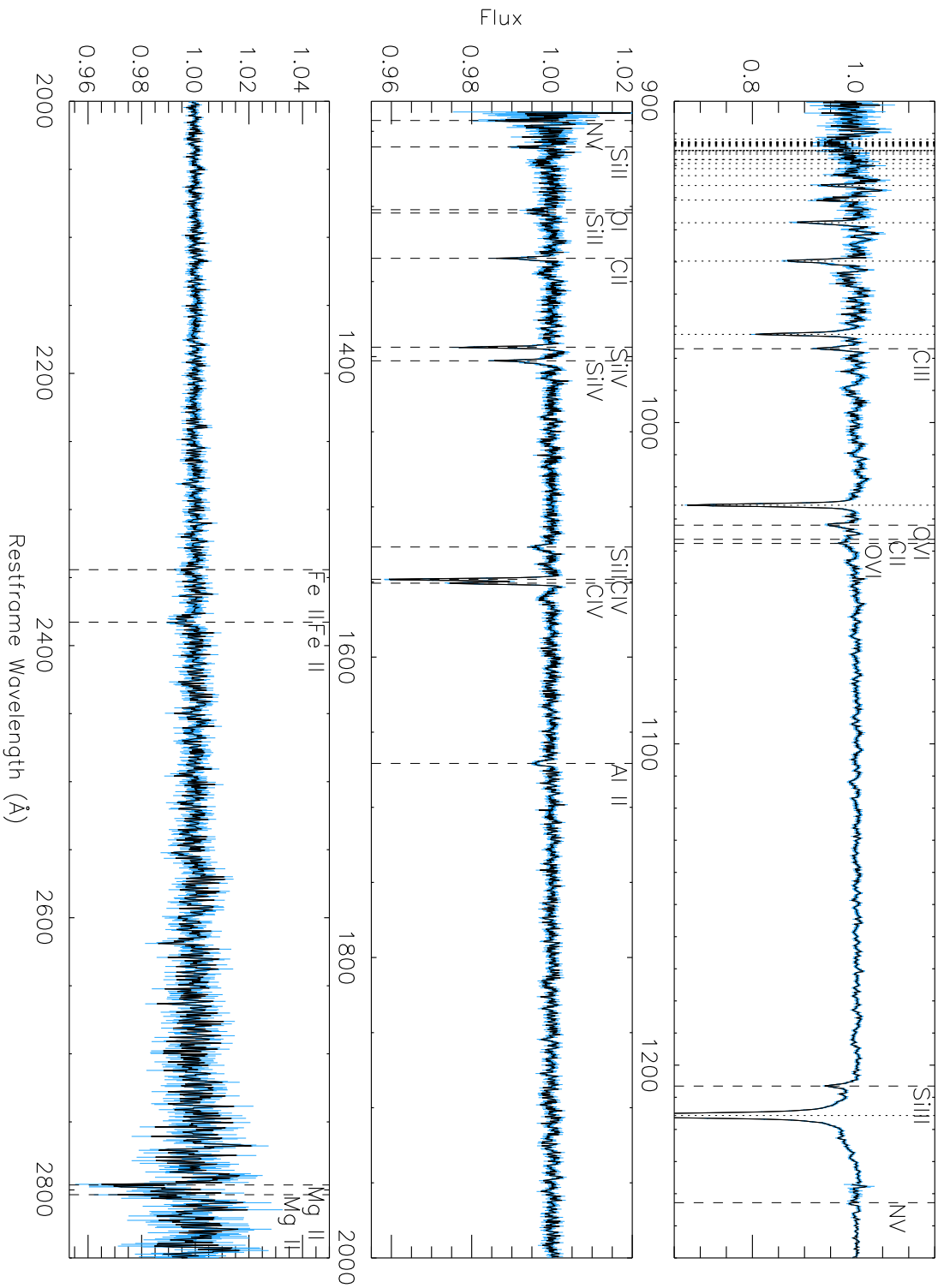

FIG. 2.— The rest-frame spectrum of our selected Lyα absorbers. The blue vertical lines indicate the error estimate. This composite is produced by scaling away the 'pseudo- continuum' from the median stacked spectrum shown in Figure 1. Lyman series lines are marked (*dotted lines*). Metal lines found at high confidence are marked (*dashed lines*) with labels to the right. These metal lines have been fitted and the results of these fits are shown in Table 1. Note the difference in scales for both axes for all panels.

3. LINE FITTING AND INTERPRETATION

Full interpretation of these stacked spectra will require the use of model spectra and/or degraded high-resolution spectra to account for the effects of line blending, sample selection, and pseudo-continuum subtraction. In this paper, we restrict our interpretation to some general conclusions that can be drawn by comparing the measured line strengths to simple models.

3.1. *H I Column Density*

Figure 3 shows a measurement of the H I column density using the Lyman series. For each of seven Lyman series lines (n=1:Lyα, n=2:Lyβ, n=3:Lyγ etc.), we measure a rest-frame equivalent width W. We plot them normalized by the product $f\lambda$ of oscillator strength and line wavelength. Optically thin Lyman series lines would all have equal values of $W/f\lambda$. The equivalent width is shown for both the median and the arithmetic mean, with error bars drawn from bootstrapping in the composite spectra. The noise in the arithmetic mean spectrum renders the pseudo-continuum fitting blueward of 935Å unreliable, so we only show Lyman lines n=1,2,3,4 and 5.

The curves in Figure 3 are created by using VPFIT[7] to generate model lines at SDSS resolution, from which we measure a simulated W. The flatness of the $n = 4-7$ points in the median stack suggests that these lines are optically thin, and comparison to the model curves then implies a total column density $\log N_{\rm HI}/{\rm cm}^{-2} \approx 15.3 - 15.5$ for our median absorption features. In this column density range, lines with velocity width $b = 30\,{\rm km\,s}^{-1}$ go from significantly saturated at $n = 3$ to minimally saturated at $n = 4$, in agreement with the trend in the data points. Lines with $b = 15\,{\rm km\,s}^{-1}$, corresponding to the narrowest Doppler parameters seen for individual Lyα forest absorbers, predict rising values of $W/f\lambda$ from $n = 4-7$, in clear disagreement with the observed trend. Lines much broader than $b = 30\,{\rm km\,s}^{-1}$ would predict too much Lyβ and Lyγ absorption relative to the higher order lines.

Of course, these absorption features are probably not well described by single Voigt line profiles, in part because the composite spectrum comes from systems with a range of properties, but mostly because the contributing features are themselves blends of multiple lines. The models in Figure 3 all under-predict the Lyα equivalent width, plausibly because the "main" absorption feature is near-saturated in Lyα and absorption outside the Gaussian wings (but still within the SDSS resolution element) makes a larger relative contribution. While the b parameters implied by Figure 3 have a complex and non-trivial significance, the high-order Lyman series lines do appear to give a robust estimate of the total column density characteristic of our median stack, with $\log N_{\rm HI}/{\rm cm}^{-2} \approx 15.3 - 15.5$. Results for the arithmetic mean stack suggest a column density lower by 0.1-0.2 dex, but it is harder to draw clear conclusions because we cannot robustly measure Lyman-6 and Lyman-7 in the arithmetic mean stack.

3.2. *Metal line Column Densities*

[7] http://www.ast.cam.ac.uk/ ∼rfc/vpfit.html

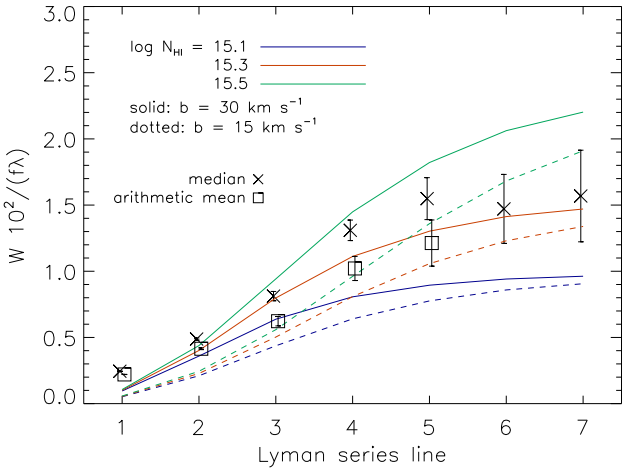

FIG. 3.— Curve of growth for the first seven Lyman series lines, labelled 1 (Lyα) to 7 (Lyη). Points show the rest-frame equivalent widths normalized by $f\lambda$ measured from the median stack (*crosses*) and the arithmetic mean stack (*squares*). Curves show predictions for Gaussian lines with b-parameters of $30\,{\rm km\,s}^{-1}$ (*solid*) and $15\,{\rm km\,s}^{-1}$ (*dashed*) and column densities $\log N_{\rm HI}/{\rm cm}^{-2} = 15.1$, 15.3, 15.5 (bottom to top).

We have used VPFIT to fit all of the metal lines marked in Figure 2, assuming spectral resolution $R = 2000$. Wherever possible, we measure each line independently. Only the blended transitions C II with the weaker O VI line, along with O I and one of our Si II lines (λ1304), are fitted with a joint analysis. Since contamination by Si III shadowing is a concern for the weaker Si IV line we discard it from the analysis. Table 1 lists the rest wavelengths, equivalent widths (W) and the fitted column densities (N), Doppler parameters (b), and reduced χ^2 values for both the median and arithmetic mean stacks. Many lines have fitted b-parameters significantly larger than the expected width of metal lines. There is a large scatter in widths but low ionization lines are typically broader. These large velocity widths could be a signature of dispersion within the absorption systems or large-scale clustering of the metal lines with the Lyα absorbers (which is consistent with the Lyα clustering signal). These results are in line with measurements of C IV clustering on scales of up to 600 ${\rm km\,s}^{-1}$ (Pieri et al. 2006; Scannapieco et al. 2006).

Regardless of the true line widths, these metal lines are likely to be optically thin, making the derived column densities robust within the VPFIT-derived errors. Multiple measurements of the same species for a given stack are usually consistent within quoted errors, with the notable exceptions of Si II and C IV. In the case of Si II, the line at 1260Å is discrepant with the other two measured lines. The continuum varies rapidly over a narrow wavelength range in this part of the spectrum, and we conclude that the continuum fitting for this line is the dominant source of error and therefore drop the line from further analysis. The two lines of the C IV doublet imply column densities that differ by 0.1 dex, about five times the quoted 1σ errors. Also, the fit for the strongest doublet member is poor. Since this is the strongest metal line, it may also have the strongest signal of clustering in the line profile, violating the single-line model assumption used in VPFIT. We conclude that the precision of this measurement is at the 0.1 dex level.

Figure 4 shows our column density measurements from the median and arithmetic mean stacks. Species are listed in order of decreasing ionization potential. The column densities derived from the mean stack tend to be slightly higher, by about 0.2 dex, but the overall agreement is good. Somewhat counter-intuitively, the similarity of line strengths in the arithmetic mean and median stacks does not imply that this level of absorption is present in most selected absorbers. If the individual lines are not outliers with respect to the noise distribution, then a sub-population of absorbers can shift the mean and median flux decrements by similar amounts. By looking at the full distribution of flux decrements, one can set limits on the fraction of systems that contribute most of the absorption. While we reserve detailed analysis to future work, our preliminary studies of the distribution of flux decrements at line center suggests that the metal lines with higher ionization potentials (for Si III and greater) arise in 15–30% of the selected Lyα systems and that the lower ionization lines (for C II and lower) arise in 5–15% of systems.

Despite this caveat about sample inhomogeneity, it is useful to compare our results with the simple predictions. Model curves are shown in Figure 4 using CLOUDY version 08.00 (Ferland et al 1998), and assuming $\log N_{\rm HI} = 15.4$, a solar abundance pattern and a quasar+galaxy UV background (Haardt & Madau 2001). Four curves show a range of models representing typical conditions in the Lyα forest with a metallicity of [Fe/H]$= -2$. Physical conditions $\rho/\bar{\rho} \approx 10$ and $T = 10^4 - 10^{4.5}$ K give a reasonable match to the high-ionization lines, but the strengths of the lower ionization lines are underpredicted by two orders of magnitude or more. Therefore, lower ionization potential species are unlikely to be reproduced by models with diffuse IGM conditions. We can, however, get an approximate match to these lines with $\rho/\bar{\rho} \sim 1000$, $T \approx 10^4$ K, and near-solar metallicities. Since the H I column densities implied by the Lyman-series lines are far too low for self-shielding (which requires $N_{\rm HI} \gtrsim 10^{17}{\rm cm}^{-2}$), the absorbing gas should be photo-ionized by the UV background, so its temperature is unlikely to be below 10^4 K.[8] The combination of these high densities with $N_{\rm HI} \approx 10^{15.4}{\rm cm}^{-2}$ implies ~ 10 pc pathlengths for these low ionization absorbers. We conclude that different absorber populations, or perhaps different gas phases within the same systems, are responsible for the high- and low- ionization lines.

The high density, high metallicity, and short pathlength implied by this analysis suggests that the low ionization metal lines may arise in circumgalactic regions, perhaps in outflows from high redshift galaxies, or perhaps in enriched filaments feeding these galaxies. The Lyα absorption features are similar to those found in sightlines that pass within ~ 100 kpc of Lyman break galaxies (Steidel et al. private communication; Steidel et al. 2009).

4. CONCLUSIONS

[8] We cannot completely rule out the possibility that the low ionization species arise in a small fraction of systems that are self-shielded (Lyman Limit systems). It is unlikely that such a model could be reconciled with the low mean depth of Lyman-series lines, but this should be investigated further.

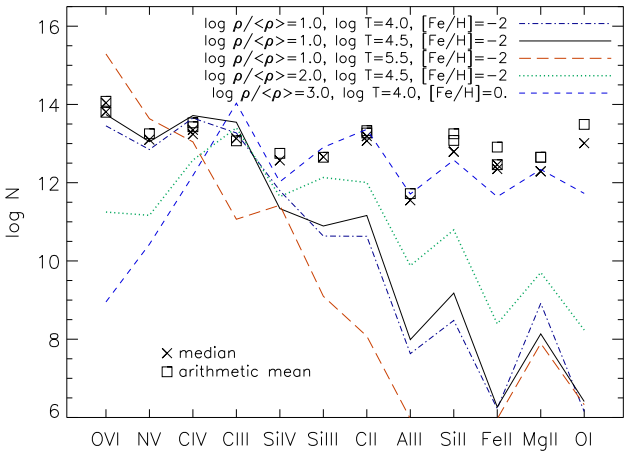

FIG. 4.— The column densities of metal species measured in order of decreasing ionization potential. Column densities from our median and mean composite spectrum are shown as crosses and squares, respectively. Models curves are shown, assuming $log N_{\rm HI} = 15.4$, a solar abundance pattern and a quasar+galaxy UV background. The $\rho/\bar{\rho} \sim 1000$ model curve is an example of clumpy conditions and the other curves represent densities and temperatures typical of the IGM as probed by the Lyα forest at high redshift.

We have developed a technique for measuring the *composite spectrum of Lyα forest absorbers* and applied it to 13,279 quasar spectra from the SDSS. From our stacked spectra, we measure equivalent widths of Lyman series lines up to $n = 7$ and column densities of 19 metal lines. We find metal lines from species previously detected in the Lyα forest (O VI, N V, C IV, C III, Si IV and Si III), from new ionization states of oxygen (O I), silicon (Si II), and carbon (C II), and from new elements magnesium (Mg II), aluminum (Al II) and iron (Fe II) not previously identified in high-redshift Lyα forest studies. Consistent results from the median and arithmetic mean stacked spectra and from multiple lines of the same ionic species show that the measured column densities are robust. High b-parameters of the fitted metal lines provide a suggestive signal of large-scale clustering or high velocity dispersions in the environment of the absorbers.

Analysis of the Lyman series implies typical column densities $N_{\rm HI} \approx 10^{15.4}{\rm cm}^{-2}$ for systems in our median stack. The high-ionization metal-line species can then be explained assuming typical physical conditions for the diffuse IGM and metallicity [Fe/H]≈ -2, but reproducing the low-ionization species requires much higher metallicities and higher densities, probably arising in a minority sub-population of the absorption systems.

The composite spectrum technique introduced here has the potential to teach us a great deal about physical conditions and enrichment of the IGM and the spectral shape of the ionizing background radiation. A natural next step is to compare composite spectra in narrower bins of redshift and Lyα optical depth, and to apply the technique to the weaker but more abundant Lyα forest absorbers that dominate the mean opacity. In this regard, we note that the high-redshift quasar sample from the Baryon Oscillation Spectroscopic Survey of SDSS-III (Schlegel et al. 2009) will eventually exceed the size of the current SDSS sample by an order of magnitude. This technique may also be usefully applied to high-resolution spectra and to *Hubble Space Telescope* spectra of the low-

TABLE 1
Metal lines measured in the composite rest-frame spectrum of Lyα absorbers

Species	λ(Å)	Median				Arithmetic mean			
		$logN$	$b(\mathrm{km\,s^{-1}})$	χ^2_r (dof)	W (mÅ)	$logN$	$b(\mathrm{km\,s^{-1}})$	χ^2_r (dof)	W (mÅ)
C II[a]	1036	13.2 ± 0.4	400 ± 300	1.1(22)	91 ± 8	13.3 ± 0.2	300 ± 200	1.3 (22)	103 ± 6
C II	1335	13.07 ± 0.04	260 ± 30	1.0 (9)	22 ± 2	13.33 ± 0.02	320 ± 20	0.64 (9)	38 ± 2
C III	977	13.13 ± 0.03	170 ± 20	0.79 (14)	79 ± 9	13.07 ± 0.06	250 ± 40	1.4 (14)	64 ± 9
C IV	1548	13.24 ± 0.02	160 ± 10	5.3 (8)	66 ± 1[c]	13.43 ± 0.02	180 ± 10	6.7 (8)	100 ± 2[c]
C IV	1551	13.35 ± 0.01	158 ± 6	0.24 (5)	20 ± 1[c]	13.53 ± 0.01	179 ± 9	1.2 (5)	50 ± 1[c]
N V	1243	13.1 ± 0.4	150 ± 20	0.87 (17)	9 ± 7	13.2 ± 0.1	210 ± 80	0.73 (17)	14 ± 8
O I[b]	1302	13.0 ± 0.1	210 ± 70	1.0 (19)	16 ± 2	13.49 ± 0.08	380 ± 80	0.85 (19)	42 ± 3
O VI	1032	13.81 ± 0.05	210 ± 30	1.6 (7)	76 ± 5	13.80 ± 0.05	250 ± 40	2.9 (7)	68 ± 3
O VI[a]	1038	14.0 ± 0.1	450 ± 60	1.1(22)	91 ± 8	14.1 ± 0.3	550 ± 50	1.3 (22)	103 ± 6
Mg II	2796	12.3 ± 0.2	200 ± 100	1.7 (7)	80 ± 20	12.6 ± 0.1	300 ± 100	2.5 (7)	150 ± 20
Mg II	2804	$12. \pm 5.$	< 600	0.98 (8)	50 ± 20	12.7 ± 0.3	300 ± 100	0.80 (8)	70 ± 20
Al II	1671	11.55 ± 0.04	330 ± 40	0.56 (11)	14 ± 1	11.72 ± 0.03	380 ± 40	0.69 (11)	20 ± 1
Si II	1260	11.88 ± 0.07	200 ± 50	0.95 (14)	10 ± 3	12.39 ± 0.06	450 ± 90	1.5 (14)	37 ± 3
Si II[b]	1304	12.8 ± 0.1	230 ± 70	1.0 (19)	16 ± 2	13.3 ± 0.1	700 ± 200	0.85 (19)	42 ± 3
Si II	1527	12.80 ± 0.05	450 ± 60	0.69 (16)	16 ± 2	13.08 ± 0.05	580 ± 80	1.4 (16)	27 ± 2
Si IV	1394	12.57 ± 0.01	140 ± 8	0.52 (6)	31 ± 1	12.75 ± 0.01	174 ± 7	0.49 (6)	46 ± 1
Si III	1207	12.66 ± 0.02	220 ± 20	0.89 (10)	69 ± 4	12.65 ± 0.01	253 ± 8	0.99 (10)	66 ± 3
Fe II	2344	12.5 ± 0.3	500 ± 300	1.0 (13)	11 ± 5	12.9 ± 0.3	< 1000	1.3 (13)	22 ± 5
Fe II	2383	12.35 ± 0.09	500 ± 100	0.76 (19)	37 ± 7	12.46 ± 0.08	420 ± 90	1.3 (19)	49 ± 7

[a] Lines fitted together as a blend and equivalent width measured together.
[b] Lines fitted together as a blend and equivalent width measured together.
[c] Partial blend so blended portion not included in equivalent width measurement.

redshift Lyα forest, using the power of large numbers to bring out features that are too weak to appear in even the best single-quasar spectra.

We thank Jason X. Prochaska and Richard Pogge for useful discussions, and Benjamin Oppenheimer for the use of his CLOUDY output tables. MP is supported in part by the Center for Cosmology and Astro-Particle Physics at Ohio State University. DW gratefully acknowledges the support of an AMIAS membership at the Institute for Advanced Study.

Funding for the SDSS and SDSS-II has been provided by the Alfred P. Sloan Foundation, the Participating Institutions, the NSF, the US Department of Energy, the National Aeronautics and Space Administration (NASA), the Japanese Monbukagakusho, the Max Planck Society, and the Higher Education Funding Council for England. The SDSS Web site is at http://www.sdss.org/.

REFERENCES

Adelman-McCarthy, J. et al. 2007, ApJS, 172, 634
Aguirre, A., Schaye, J., Kim, T.-S., Theuns, T., Rauch, M., & Sargent, W. L. W. 2004, ApJ, 602, 38
Aguirre A., Dow-Hygelund C., Schaye J., & Theuns, T. 2008, ApJ, 689, 851
Bergeron, J., & Herbert-Fort, S. 2005, (astro-ph/0506700)
Cowie, L. L., & Songaila, A., Kim, T.-S. , & Hu, E., M. 1995, AJ, 109, 1522
Cowie, L. L., & Songaila, A. 1998, Nature, 394, 44
Ellison, S. L., Songaila, A., Schaye, J., & Pettini, M. 2000, ApJ, 120, 1175
Fechner, C., Richter, P. 2009, A&A, 496, 31
Ferland, G. J., Korista, K. T., Verner, D. A., Ferguson, J. W., Kingdon, J. B., & Verner, E.M. 1998, PASP, 110, 761
Frank, S., Mathur, S., Pieri M., & York, D. 2009, AJ in press (astro-ph/0707.1700)
Haardt, F. & Madau, P. 2001, in Clusters of Galaxies and the High Redshift Universe Observed in X-rays, ed. Neumann, D. M. & Tran, J. T. V., (astro-ph/0106018) (HM01)
Mac Low, M.-M., & Ferrara, A. 1999, ApJ, 513, 142
Madau, P., Ferrara, A., & Rees, M. J. 2001, ApJ, 555, 92
Meyer, D. M., & York, D. G. 1987, ApJ, 315, L5
McDonald, P., Seljak, U., Burles, S., Schlegel, D. J., Weinberg, D. H., Cen, R., Shih, D., Schaye, J., Schneider, D. P., Bahcall, N. A., Briggs, J. W., Brinkmann, J., Brunner, R. J, Fukugita, M., Gunn, J. E., Ivezić, Ž., Kent, S., Lupton, R. H.,& Vanden Berk, D. E. 2006, ApJS, 163, 80
Nestor, D. B., Turnshek, D. A., & Rao, S. M. 2005, ApJ, 628, 637
Oppenheimer, B. D., & Davé, R. 2006, MNRAS, 373, 1265
Pieri, M. M., & Haehnelt, M. G. 2004, MNRAS, 347, 985
Pieri, M. M., Schaye, J., & Aguirre, A.,ApJ, 638, 45
Pieri, M. M., Martel, H., & Grenon, C. 2007, ApJ, 658, 36
Pieri, M. M. & Martel, H. 2007, ApJ, 662, 36, L7
Pieri, M. M., Frank, S., Mathur, S., Weinberg, D., H., York, D. G., & Oppenheimer, B., D., 2010, ApJ, 716, 1084
Scannapieco, E., Pichon, C., Aracil, B., Petitjean, P., Thacker, R. J., Pogosyan, D., Bergeron, J., & Couchman, H. M. P. 2006, MNRAS, 365, 615
Schaye, J., Rauch, M., Sargent, W. L. W., & Kim, T.-S. 2000, ApJ, 541, L1
Schaye, J., Aguirre, A., Kim, T.-S., Theuns, T., Rauch, M., & Sargent, W. L. W. 2003, ApJ, 596, 768
Schlegel D., White M., & Eisenstein D. 2009, arXiv:0902.4680
Simcoe R. A, Sargent W. L. W., & Rauch, M. 2004, ApJ, 606, 92
Steidel, C., Martin, C., Prochaska, J. X., Pettini, M., Schaye, J., Rakic, O. 2009, Astro2010, White Paper no. 286

Songaila, A., & Cowie, L. L. 1996, AJ, 112, 335
York, D. G, Khare, P., Vanden Berk, D., Kulkarni, V. P., Crotts, A. P. S., Lauroesch, J. T., Richards, G. T., Schneider, D. P., Welty, D. E., Alsayyad, Y., Kumar, A., Lundgren, B., Shanidze, N., Smith, T., Vanlandingham, J., Baugher, B., Hall, P. B., Jenkins, E. B., Menard, B., Rao, S., Tumlinson, J., Turnshek, D., Yip, C.-W., & Brinkmann, J. 2006, MNRAS, 367, 945